

Effectiveness of regional diffusion MRI measures in distinguishing multiple sclerosis abnormalities within the cervical spinal cord

Haykel Snoussi^{a,1,*}, Julien Cohen-Adad^b, Benoît Combès^a, Élise Bannier^{a,c}, Slimane Tounekti^d, Anne Kerbrat^e, Christian Barillot^a, Emmanuel Caruyer^{a,*}

^aUniv Rennes, CNRS, Inria, Inserm, IRISA UMR 6074, Empenn ERL U 1228, Rennes, France

^bNeuroPoly Lab, Institute of Biomedical Engineering, Polytechnique Montreal, Montreal, Canada

^cDepartment of Radiology, Rennes University Hospital, Rennes, France

^dDepartment of Radiology, Thomas Jefferson University, Philadelphia, PA, USA

^eDepartement of Neurology, Rennes University Hospital, Rennes, France

Abstract

Multiple sclerosis is an inflammatory disorder of the central nervous system. Quantitative MRI has huge potential to provide intrinsic and normative values of tissue properties useful for diagnosis, prognosis and ultimately clinical follow-up of this disease. However, there is a large discrepancy between the clinical observations and how the pathology is exhibited in MRI brain scans. Complementary to brain imaging, the study of multiple sclerosis lesions in the spinal cord has recently gained interest as a potential marker for early physical impairment. Therefore, investigating how the spinal cord is damaged using quantitative imaging, in particular, diffusion MRI, becomes an acute challenge. In this work, we extract average diffusion MRI metrics per vertebral level from spinal cord data acquired from multiple clinical sites. The diffusion-based metrics involved are extracted from the diffusion tensor imaging and Ball-and-Stick models and quantified for every cervical vertebral level using a collection of image processing methods and an atlas-based approach. Then, we perform a statistical analysis study to characterize the feasibility of these metrics to detect lesions. Specifically, we study the usefulness of combining different metrics to improve the accuracy prediction score associated with the presence of multiple sclerosis lesions. We demonstrate the grade of sensitivity to underlying microstructure changes in MS patients of each metric. Ball-and-Stick provides novel information about the MS damage to tissue microstructure. In addition, we show that choosing a subset of metrics: [FA, RD, MD] and [FWW, MD, Stick-AD, RD], which bring complementary information, has significantly increased the prediction score of the presence of the MS lesion in the cervical spinal cord.

Keywords: Diffusion MRI, Statistical Analysis, Spinal Cord, Multiple Sclerosis

1 Introduction

Multiple sclerosis (MS) is an inflammatory and neurodegenerative disease that affects the central nervous system (CNS) and leads to severe neurological dysfunction as well as cognitive and physical incapacitation. It is characterized by the presence of focal lesions, neuroaxonal loss and damage to the brain, the spinal cord and the optic nerves [Inglese and Bester \(2010\)](#); [Wheeler-Kingshott et al. \(2014\)](#). In patient with MS, the spinal cord is considered as an important clinically eloquent structure. The damage to specific spinal cord tracts is strongly

associated with the disability and the functional deficits in patients with MS [By et al. \(2017\)](#). Spinal cord lesions are frequent in the cervical part, commonly restricted to two vertebral levels in length, fill less than half of the cross-sectional area of the spinal cord and generally peripheral [Bot and Barkhof \(2009\)](#); [Stroman et al. \(2014\)](#). A variety of MS spinal cord pathological abnormalities, including demyelination are widely investigated in vivo using advanced imaging techniques such as the magnetic resonance imaging (MRI). MRI techniques, including diffusion-weighted imaging, magnetization transfer, spectroscopy imaging and functional MRI allow the detection of the tissue changes and provide a valuable prognostic information even in early stage of MS. Therefore, MRI has become a fundamental tool for the diagnosis and follow-up of MS patient and for the monitoring of the disease evolution as well as the treatment response assessment [Amélie et al. \(2015\)](#).

Although the widespread use of the conventional MRI in MS monitoring, it remains limited to describe the entire spectrum of the disease process that give rise to the clinical manifestations. Conventional MRI shows little correlation with histological findings and clinical disability of the MS patients [Barkhof \(2002\)](#); [Inglese and Bester \(2010\)](#). This clinical–radiological

*Correspondence: Haykel Snoussi, Glenn Biggs Institute for Neurodegenerative Disorders, University of Texas Health Science Center at San Antonio, San Antonio, Texas, USA. Emmanuel Caruyer, Univ Rennes, CNRS, Inria, Inserm, IRISA UMR 6074, Empenn ERL U 1228, Rennes, F-35000

Email addresses: dr.haykel.snoussi@gmail.com (Haykel Snoussi), Emmanuel.Caruyer@irisa.fr (Emmanuel Caruyer)

¹Haykel Snoussi was partly funded by the EMISEP PHRC, the Brittany region and a MITACS-Inria Globalink travel grant. MRI data acquisition was supported by the Neurinfo MRI research facility, University of Rennes 1. Neurinfo is granted by the the European Union (FEDER), the French State, the Brittany Council, Rennes Metropole, Inria, Inserm and the University Hospital of Rennes 1.

mismatch is mainly due to several drawbacks, including their low sensitivity to diffuse tissue. It has been shown that these techniques are unable to detect and quantify the extent of tissue injury within macroscopic lesions in the normal-appearing cord of patients with MS [Filippi and Grossman \(2002\)](#); [Rovaris et al. \(2006\)](#). Therefore, there is a need to assess spinal cord involvement in MS with more advanced imaging techniques. These techniques should be able to reveal more aspects about the mechanism associated with tissue changes in order to understand the underlying pathology.

Diffusion imaging has recently shown its potential to provide intrinsic and normative value to tissue properties useful for diagnosis, prognosis and ultimately clinical trials in MS [Agosta et al. \(2007a\)](#); [Inglese and Bester \(2010\)](#). Various studies investigated the correlation between the presence of MS lesion and diffusion-based metrics [Hesseltine et al. \(2006\)](#); [von Meyenburg et al. \(2013\)](#); [Miraldi et al. \(2013\)](#). For example, [Agosta et al. \(2007a\)](#) showed that one of Diffusion Tensor Imaging (DTI) metric, mean diffusivity, increases within C2 and C3 vertebral levels of MS patients. However, performing diffusion MRI on the spinal cord is technically challenging due to various considerations related to the spinal cord anatomy, location and to the MRI limitations [Snoussi et al. \(2019\)](#). In fact, diffusion MRI is known by its low-spatial-resolution and its-high sensitivity to motion. Hence, DTI maps are typically affected by the complex intravoxel tissue properties, which reduces the specificity of the derived metrics to the different pathological features of MS.

Few limited studies developed and investigated advanced diffusion models such as Diffusion Kurtosis Imaging (DKI) and Neurite Orientation Dispersion and Density Imaging (NODDI) to provide better sensitivity and specificity to the underlying properties of the damaged tissue in spinal cord [Grussu et al. \(2015\)](#); [By et al. \(2017\)](#). In fact, the application of these multi-compartment models in the spinal cord requires a high b-value and high number of diffusion encoding directions, resulting in insufficient signal-to-noise-ratio (SNR) and clinically unfeasible scan time. In addition, and although their important findings, the used data is very limited in terms of number of subjects and the regions' volume in which the diffusion metrics were quantified.

Therefore, the main objectives of this multicenter study are: firstly to demonstrate the feasibility of Ball-and-Stick model [Behrens et al. \(2003\)](#) in addition to the DTI model in the cervical spinal cord for patients with MS, secondly to investigate the usefulness of combing different metrics derived from these models to improve their sensitivity associated with the presence of MS lesions. Using atlas-based approach and a collection of image processing approaches, diffusion-based metrics were extracted and quantified per vertebral level. Then, a statistical analysis study including a multivariate classification was performed for the detection of MS lesions.

2 Materials and processing pipeline

2.1 Multiple sclerosis patients and healthy volunteers

This multicenter study includes 82 subjects: 29 healthy volunteers (mean age = 32.83 ± 7.13 , 18F/11M) and 53 MS patients (mean age = 32.58 ± 6.25 , 34F/19M) were recruited in the study approved by the local research ethics committee (PROJECTXXX). MS patients are early relapsing-remitting MS patients (scan within the first year following diagnosis), with a median Expanded Disability Status Scale (EDSS) score of 1.0 (range [0, 2.5]). All participants provided informed written consent. Healthy volunteers and MS patients are from 4 hospitals in *****: Center 1, Center 2, Center 3 and Center 4. [Table. 1](#) reports details about MRI scanners, centers and subjects' characteristics.

2.2 MRI Acquisition

Scans were acquired on Siemens 3T MRI scanners (Verio and Skyra). Following, we give a brief presentation of each MR modality we processed. Thirty diffusion-weighted images (DWI) were acquired at $b = 900 \text{ s}\cdot\text{mm}^{-2}$ with non-collinear gradient directions, six non-DWI ($b = 0$) measurements and one non-DWI ($b = 0$) with an opposite phase encoding direction (PED) were also acquired. This was repeated three times successively in order to increase the signal-noise ratio (SNR). Scans were performed in sagittal orientation and head-feet (HF) PED. The pulse sequence used for diffusion MRI is a single-shot echo-planar imaging using parallel imaging (GRAPPA, acceleration factor 2). Sixteen slices were acquired with the following parameters without inter-slice gap: TR/TE = 3600/90 ms, with $2 \times 2 \times 2 \text{ mm}^3$ as the resolution, and image matrix 80×80 . The total acquisition time for the dMRI sequence was approximately 7 minutes. The protocol also includes three anatomical references: T_1 -weighted scan in sagittal orientation, with $1 \times 1 \times 1 \text{ mm}^3$ resolution, TR/TE = 1800/2.79 ms and FoV = 250 mm, T_2 -weighted scan in sagittal orientation, with $0.7 \times 0.7 \times 2.75 \text{ mm}^3$ resolution, TR/TE = 3000/68.0 ms and Fov = 260 mm and axial T_2 scan $0.6 \times 0.5 \times 3 \text{ mm}^3$ resolution, TR/TE = 4790/94 ms and Fov = 180 mm.

2.3 Analysis and processing pipeline

In this section, we present the processing pipeline, from the raw images to the extracted diffusion measures per subject and per vertebral level in the cervical spinal cord. To ensure that the results are immune to image artifacts, and to identify problems during the processing pipelines, we performed a careful quality control on the raw data and after each processing step. This is a crucial stage for the quality of the analysis and the accuracy of the results.

2.3.1 Image preprocessing

Motion between DWI were corrected using the method presented in [Xu et al. \(2013\)](#) and implemented in the Spinal Cord Toolbox (SCT) [De Leener et al. \(2017\)](#). Then, dMRI data were corrected for susceptibility distortion using Hyperelastic Susceptibility Artefact Correction (HySCO) method as implemented

Center	Center 1	Center 2	Center 3	Center 4	TOTAL
3T Siemens MRI	Verio	Verio	Verio	Skyra	-
Volunteers	4	18	3	4	29
Gender	F/3M	10F/8M	3F	4F	18F/11M
Mean age(year)	34.0±4.74	32.61±7.97	34.67±5.25	31.25±5.67	32.83±7.13
Mean weight(kg)	72.5 ± 6.7	65.4 ± 11.4	65.0 ± 7.5	56.0 ± 4.1	65.0 ± 10.7
Mean size(m)	1.75 ± 0.03	1.72 ± 0.09	1.66 ± 0.06	1.64 ± 0.04	1.71 ± 0.08
MS Patients	6	35	5	7	53
Gender	4F/2M	22F/13M	3F/2M	5F/2M	34F/19M
Mean age(year)	34.17±7.90	31.74±6.08	33.80±5.91	34.57±4.78	32.58±6.25
Mean weight(kg)	69.7 ± 10.5	67.9 ± 13.9	65.6 ± 6.7	69.1 ± 13.6	68.1 ± 13.0
Mean size(m)	1.68 ± 0.08	1.70 ± 0.09	1.71 ± 0.07	1.68 ± 0.06	1.70 ± 0.09
					82 (52F/30M)

Table 1: Demographic and clinical information about the participated clinical sites and for all participating subjects, healthy volunteers and MS patients in our cohort.

in Statistical Parametric Mapping (SPM) toolbox and presented in [Ruthotto et al. \(2012\)](#). HySCO had the efficient performance for diffusion MRI of spinal cord as shown in [Snoussi et al. \(2019\)](#).

Using SCT, the whole spinal cord segmentation was carried out on T_1 -weighted, as well as on the mean of DWI ($b = 900 \text{ s}\cdot\text{mm}^{-2}$) corrected for distortion. In some cases, this segmentation was ameliorated by adjusting parameters. Then, we manually identified two vertebral levels, C3 and T1, to fulfill the requirements for the registration of T_1 -weighted data to the PAM50 template [De Leener et al. \(2018\)](#).

2.3.2 Computation of diffusion-based metrics

The diffusion-weighted signal in white matter was modeled in the spinal cord using DTI [Basser et al. \(1994\)](#) and Ball-and-Stick model [Behrens et al. \(2007\)](#). The DTI model assumes that the probability of water molecules displacement follows a zero-mean 3D Gaussian. The diffusion tensor, directly related to the covariance matrix, is a 3×3 symmetric, positive-definite matrix. From its eigenvalue decomposition, we can extract rotation-invariant indices. We focused on the radial diffusivity (RD), the axial diffusivity (AD), the mean diffusivity (MD) and the fractional anisotropy (FA). Note that MD can be expressed as a combination of AD and RD. These DTI metrics was computed using DIPY library.

Contrary to the DTI model, the Ball-and-Stick model is a two-compartment model, where each compartment provides a normalized MR signal S_1 and S_2 . These signal models correspond to intra- and extra-axonal diffusion, respectively. For the intra-axonal compartment, S_1 refers to signals coming from water inside the axons in which the diffusion is restricted. For the extra-axonal compartment, S_2 refers to signals coming from water outside the axons.

For Ball-and-Stick model, the first compartment S_1 , is a *stick*, anisotropic component, which has fiber direction \mathbf{n} and diffusivity d as parameters [Behrens et al. \(2003\)](#). The *stick* compartment describes diffusion in an idealized cylinder with

zero radius. The signal for this component is:

$$S_1(d, \mathbf{n}; b, G) = \exp(-bd(\mathbf{n} \cdot \mathbf{G})^2), \quad (1)$$

where b is the diffusion-weighting parameter and \mathbf{G} is the gradient direction. The second compartment S_2 , called a *ball*, is an isotropic component which has only the diffusivity d_0 as parameter in its signal described as:

$$S_2(b) = \exp(-bd_0). \quad (2)$$

In our implementation, we fixed λ_2 and λ_3 of the *stick* to $0.2 \times 10^{-3} \text{ mm}^2/\text{s}$ and d_0 to $3.0 \times 10^{-3} \text{ mm}^2/\text{s}$, which corresponds to the free diffusion coefficient of water. The signal model is therefore:

$$S(d, \mathbf{n}, f; b, G) = (1 - f)S_1(d, \mathbf{n}; b, G) + fS_2(b).$$

The parameters of interest that we extracted from the Ball-and-Stick model are f , the free water weight (FWW), and d , the stick axial diffusivity (Stick-AD).

2.3.3 Quantification of metrics per vertebral level

In order to compute the mean of the presented metrics for each vertebral level, we followed a processing pipeline to align the labels defined in the PAM50 template [De Leener et al. \(2018\)](#) to the native DWI space of each subject.

First, the T_1 -weighted anatomical image was registered to the PAM50- T_1 spinal cord template [De Leener et al. \(2018\)](#); this generates a forward and inverse warping field between them. Next, the PAM50- T_1 template [De Leener et al. \(2018\)](#) was registered to the mean DWI using the inverse warping field from previous registration as an initial warping field. This registration was made using T_1 -weighted instead of T_2 -weighted since its isotropic resolution made the registration more effective.

Therefore, alignment with the template provides robust definition of the inter-vertebral levels for the spine. This enables computation of the average metrics in spinal cord using the

atlas-based approach introduced in Lévy et al. (2015). As a result, we can quantify diffusion-based metrics averaged for each vertebral level in cervical part. Especially for scalar metrics, we quantify them only in white matter referring to PAM50 template. The processing pipeline is summarized in Figure. 1.

2.3.4 Ground truth: Segmentation of MS lesion

For the 53 MS patients, the MS lesions were segmented manually by 9 raters including radiologists and experienced readers as described in REFERENCEXXX. In brief, MS lesions were segmented using both axial T₂ and sagittal T₂-weighted using ITKSNAP Toolbox 3.6.0 Yushkevich et al. (2006). From these lesions masks, we computed for each vertebral level: (i) the number of MS lesions within the vertebral level, (ii) the total volume of lesions, normalized by the volume of the corresponding vertebral level. In Figure. 2, red bars report the quantity and the distribution of lesion's volume's volume in [C1-C7] region, as a reference to C1, ..., C7 levels.

3 Statistical analysis

From the processing pipeline described above, we obtained 6 diffusion-based metrics: FWW, Stick-AD, AD, FA, MD and RD. All metrics quantified and averaged to every vertebral level of every subject in our cohort. In this section, we present our proposed statistical analysis study between MS patients and healthy volunteers, for each metric separately.

3.1 Pairwise comparisons

Our cohort is composed of 29 healthy volunteers and 53 MS patients with 139 segmented lesions with different volume's size and shared in 7 vertebral level. This sample size is relatively small compared to the number of the extracted metrics, and the volume of the vertebral level in which we computed the average of the proposed metrics.

In addition and classically, such statistical analysis could be done for each vertebral level separately because of the anatomy variety within the cervical spinal cord.

Therefore, we studied the opportunity to pool the data from several vertebral levels for the purpose of increasing the statistical power of our analysis. To do so, we performed a two-way analysis of variance between vertebral levels for each metric to illustrate the interaction term between them. We compare all pairs of vertebral levels of one subject, for each level of all the other subjects. This test reveals the degree to which one subject is deferentially effective at each vertebral level of a second subject. This test was performed using the Estimated Marginal Means (EMMs), sometimes called least-squares means, which are predictions from a linear model over a reference grid; or marginal averages thereof.

Figure. 3 illustrates graphically this comparison for the 6 diffusion metrics, 4 from DTI and 2 from Ball-and-Stick, computed only on the 29 healthy volunteers data. Figure. 3 summarizes intervals of vertebral levels in which there is no significance difference. We remark that for all metrics, the [C2-C4]

region shows no significance difference. This leads to the possibility of merging metrics quantified in C2, C3 and C4 vertebral levels and consequently increasing the available data for our statistical analysis. Figure. 2 reports the quantity and the distribution of lesion's volume in [C2-C4] region comparing to [C1-C7].

3.2 Unpaired *t*-test between healthy volunteers and MS patients

We perform Welch's *t*-test between healthy volunteers and MS patients data in [C2-C4] region. This *t*-test is an adaptation of Student's *t*-test and is more reliable when the two samples have unequal variances and/or unequal sample sizes. It is often referred to as *unpaired* or *independent samples t*-tests. In this statistic test, for each metric, m_i we have the following:

$$\mathcal{V}_i = \left[h_1 \left[m_i(c_2), m_i(c_3), m_i(c_4) \right], \dots, h_{29} \left[m_i(c_2), m_i(c_3), m_i(c_4) \right] \right]$$

$$\mathcal{N}\mathcal{A}\mathcal{W}\mathcal{M}_i = \left[p_1 \left[m_i(c_j) \right], \dots, p_{53} \left[m_i(c_j) \right] \right]; c_{j \in (2,3,4)}$$

$$\mathcal{M}\mathcal{S}_i(thr) = \left[p_1 \left[m_i(c_j) \right], \dots, p_{53} \left[m_i(c_j) \right] \right]; c_{j \in (2,3,4)}$$

where, h refers to healthy volunteer, p refers to MS patient, m_i is the chosen metric with its index $i \in \{1, \dots, 6\}$, c_2 , c_3 and c_4 are the vertebral level, thr is the threshold of the percentage of the lesion's volume, \mathcal{V}_i : 87 (29×3) vertebral levels from 29 healthy controls, $\mathcal{N}\mathcal{A}\mathcal{W}\mathcal{M}_i$: 86 vertebral levels without detected lesion, i.e. as normal-appearing white matter (NAWM), $\mathcal{M}\mathcal{S}_i(thr\%)$: vertebral levels possess lesion with volume superior to $thr\%$ of the corresponding vertebral level volume. In order to have a reasonable statistical power in this *t*-test, we choose only 2 thresholds: $thr=5\%$ and $thr=10\%$. By the way, there is 36 and 24 vertebral levels in our cohort that possess lesion's volume superior to $thr=5\%$ and $thr=10\%$ respectively.

3.3 Machine learning for the detection of MS lesions

In this section, we propose to use and evaluate the diffusion MRI data to automatically detect the presence of a lesion. Throughout this part, we will evaluate classification results using the area under the curve (AUC) of the receiver operating characteristic curve (ROC).

3.4 Multivariate classification using diffusion metrics

3.4.1 Building linear discriminant analysis classifier

Based on a selection of metrics extracted from diffusion, we build a classifier which combines this set of features using the linear discriminant analysis (LDA) method Ripley (2002). LDA is a method used to find a linear combination of features that separates or characterizes two or more classes of objects. The resulting combination may be used as a linear classifier.

The full experience setup is summarized in Algorithm. 1. So, the data vector X_{comb} is constructed as the following:

$$X_{comb}(thr) = \left[\left[X_i(thr) \right], \dots, \left[X_j(thr) \right] \right] \quad (3)$$

where i and j are the index of the chosen metrics and thr is the threshold of the lesion's volume.

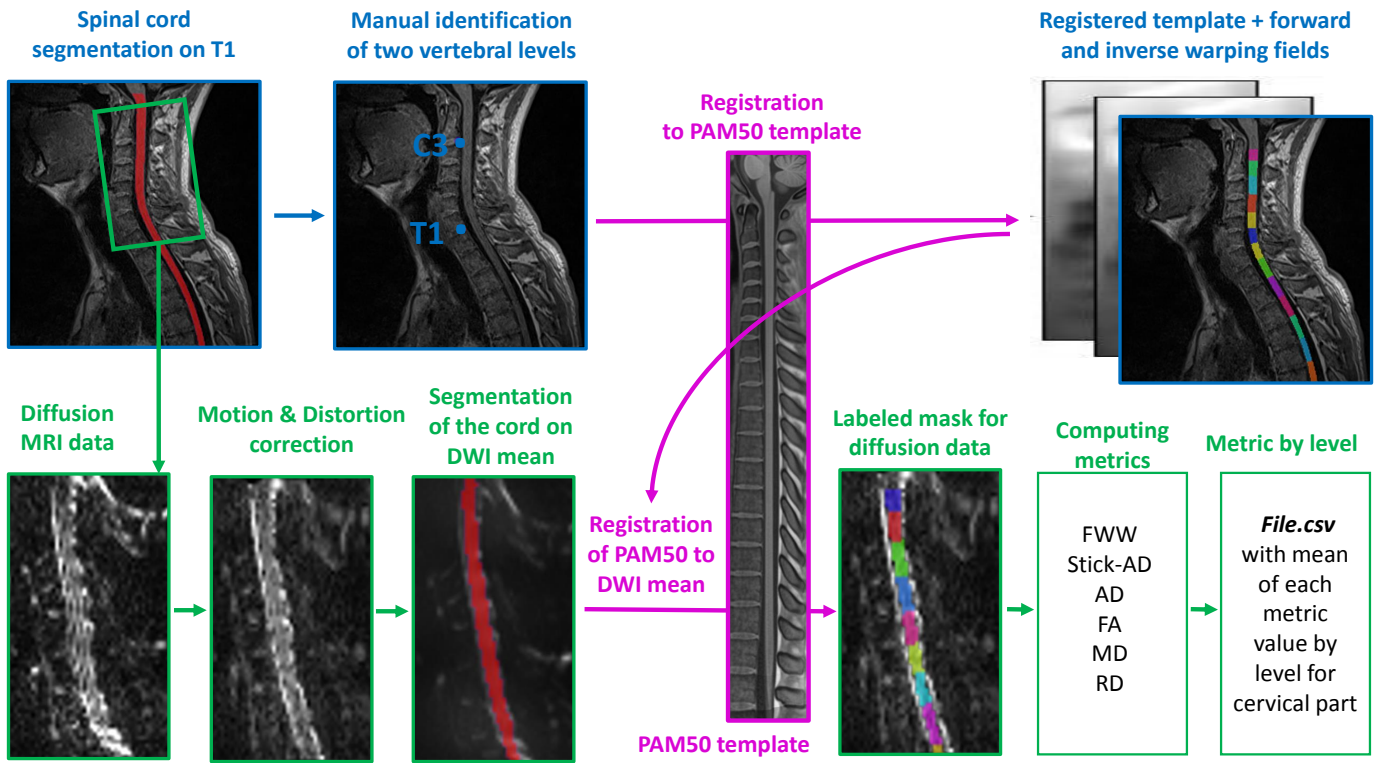


Figure 1: Illustration of the automated analysis pipeline. (1) Segmentation of the cord on T1. (2) Manual identification of two vertebral levels. (3) Registration to the PAM50 template. (4) Motion and distortion correction of dMRI data. (5) Segmentation of the cord using DWI mean data. (6) Registration of PAM50-T1 registered to DWI mean data using the inverse warping field from previous registration as an initial warping field. (7) Computing DTI and Ball&Stick metrics. (8) Quantification of metrics by vertebral level of the cervical part.

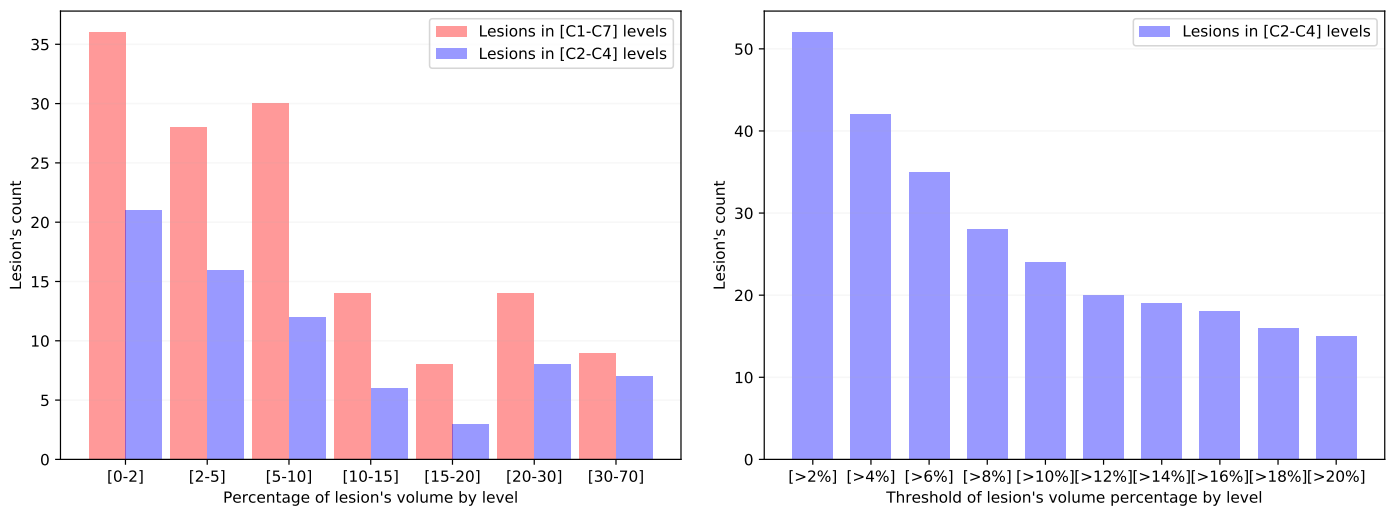


Figure 2: Left: Distribution of lesion's volume in [C1-C7] and [C2-C4] regions for several intervals of lesion's volume. Right: Distribution of lesion's volume in [C2-C4] region in 10 thresholds. Lesion's volume is the part of the vertebral volume occupied by a lesion.

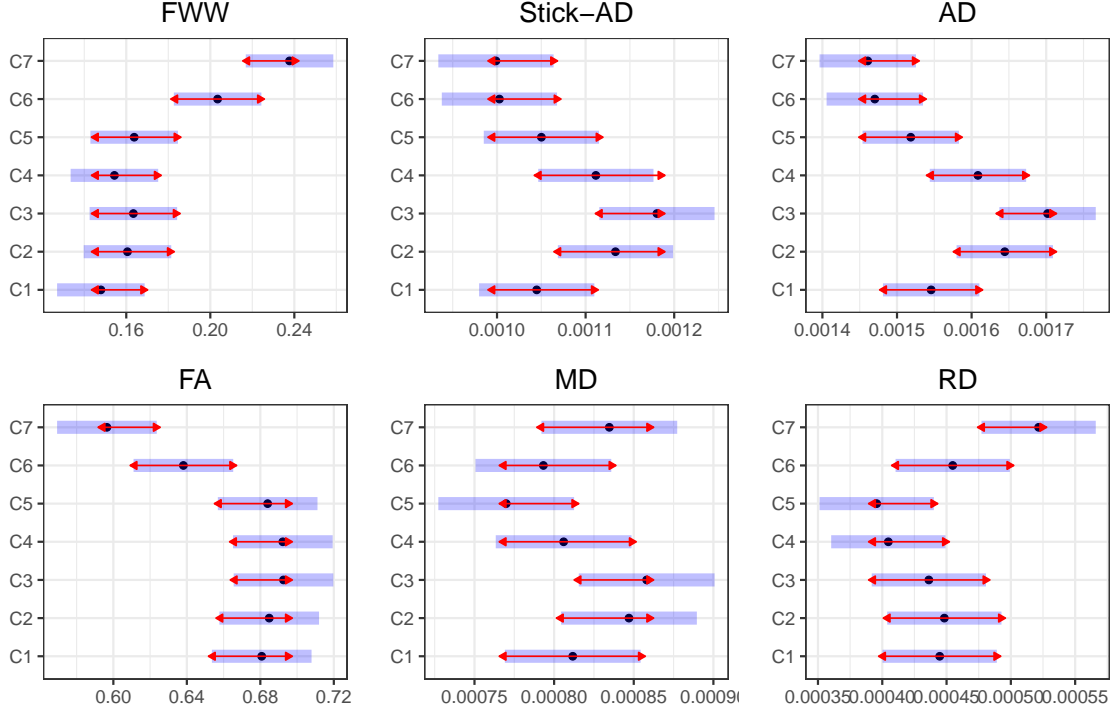


Figure 3: Estimated marginal means (x axis) for each metric in cervical vertebral levels (y axis) for healthy volunteers data. The blue bars are confidence intervals for the EMMs, and the red arrows are for the comparisons among them. If an arrow from one level overlaps an arrow from another level, the difference is not significant (p -value > 0.05). Else, the difference is significant (p -value < 0.05).

Note that depending on the threshold of the lesion’s volume, the number of vertebral level may differ in the patient group. In fact, X_{comb} contains vertebral levels of healthy volunteers (29×3) and vertebral levels of MS patients with lesions. Figure. 2 shows the count of vertebral levels having lesions for different threshold of percentage for lesion’s volume cumulatively in [C2-C4] region. This figure gives an idea about the sample size of training and testing datasets used in the following analysis. We report mean and standard deviation of ROC AUC for 1,000 splits of the dataset into training and testing parts, representing respectively 67% and 33% of the original dataset.

3.4.2 Selecting a subset of measures

As mentioned earlier, since the sample size is relatively small, we need to reduce the degrees of freedom of our linear classifier by choosing a subset of metrics. We will try to choose a subset of diffusion-based metrics that bring complementary information; to do so, we first calculate the normalized covariance matrix for all metrics in [C2-C4] region on healthy volunteers \mathcal{V} and $\mathcal{MS}(10\%)$ as shown in Figure. 4. Dark blue square shows strong correlation between 2 metrics and yellow square indicates no relationship between them. Based on these correlations, we can propose in Table 2 combinations of metrics to be studied. An important remark here is that the normalized covariance matrix presented in Figure. 4 showed a difference in correlation between some diffusion-based metrics derived from healthy and affected vertebral levels. Especially, The correla-

tion between FWW and RD decrease when metrics are quantified in MS vertebral levels. We restrict ourselves to metrics with high potential because they show good classification and present significant difference between MS patients and controls (see section 3.2).

Algorithm 1 ROC AUC for a combination of metrics

- I. Fix *threshold* of MS lesion from $\{0.02, 0.04, \dots, 0.20\}$.
 - II. Construct the data vector X_{comb} and its label vector Y_{comb} (0 to healthy volunteers and 1 to MS patients).
 - III. Standardize X_{comb} to get X_{scaled} by centering to the mean and component wise scale to unit variance.
 - IV. Split X_{scaled} 1000 consecutive times in different $X_{train}(67\%)$ and X_{test} (33%) with their corresponding Y_{train} and Y_{test} .
 - IV.1. Fit LDA using X_{train} and Y_{train} .
 - IV.2. Using the fitted LDA model, Predict confidence score on X_{test} to obtain Y_{LDA} .
 - IV.3. Compute ROC AUC score between Y_{test} and Y_{LDA} .
 - V. Calculate the mean and variance of ROC AUC scores which is computed in 1000 consecutive times.
-

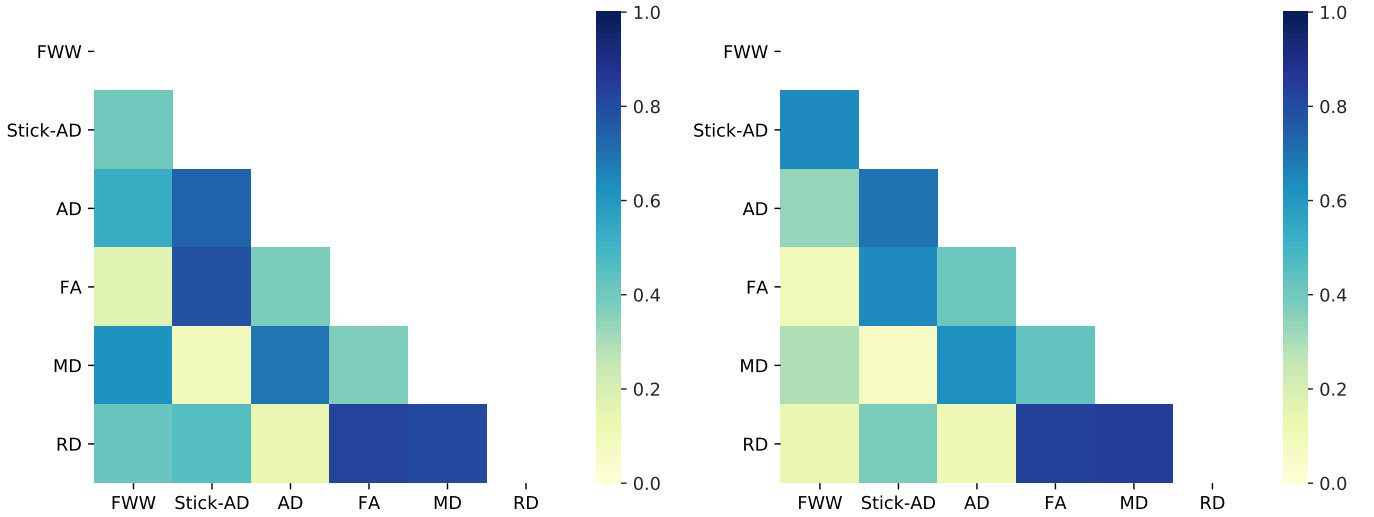


Figure 4: Normalized covariance matrix of metrics in [C2-C4] levels for healthy volunteers \mathcal{V} (left), MS patients $\mathcal{MS}(10\%)$ (right). Dark blue square shows strong correlation between the two metrics and white square indicates no relationship between them.

Subsets of 2 Metrics		Subsets of 3 and 4 Metrics			
FWW	RD	FA	MD	RD	
FWW	FA	FWW	MD	Stick-AD	
FWW	Stick-AD	FWW	MD	Stick-AD	RD
FA	MD	FWW	MD	FA	RD

Table 2: Proposed combinations of 2, 3 and 4 metrics to be studied.

4 Results

4.1 Unpaired t -test between healthy volunteers and MS patients

Table. 3 presents mean, standard deviation and p-value of each diffusion metric i between data of healthy volunteers \mathcal{V}_i , $\mathcal{N}\mathcal{A}\mathcal{W}\mathcal{M}_i$, $\mathcal{MS}_i(5\%)$ and $\mathcal{MS}_i(10\%)$ as introduced in subsection. 3.2.

FWW significantly increases in MS patients, regardless of the presence and the volume of lesions. For the second component of Ball-and-Stick model, Stick-AD, there is significant decrease on MS patients. FA shows significant decrease on MS patients who possess lesion's volume superior to 5% and 10% of the corresponding vertebral level volume. MD and RD increase significantly with MS patients with lesion's volume superior to 5% and 10%. However, for AD, there is no detectable difference between values in healthy volunteers and MS patients. Note that for this unpaired t -test between healthy and affected vertebral levels in [C2-C4] region, we fixed the threshold of the lesion's volume as a compromise with the size of available data. FWW, FA, MD and RD of MS patients still have significant difference for various threshold until the lesion's volume possess 22% of the corresponding vertebral level, but Stick-AD has a p-value < 0.05 just until 12%.

4.2 Multivariate classification using diffusion metrics

Figure. 5 presents the results of ROC AUC mean and its variance for each combination predicted by LDA and introduced in Table. 2. superposed by ROC AUC mean of each metric used in this combination. This superposition is useful since it shows whether using a combination of metrics improves on using each metric separately. The presented combinations in this part are selected and derived mainly after considering the covariance matrix, the unpaired t -test results and their ROC AUC scores.

Subset of 2 metrics: When combining FWW and Stick-AD metrics, ROC AUC mean score to separate vertebral level of controls and MS patients with lesions is better than using each metric independently. For [FWW, FA] and [FA, MD], the combination is slightly better as the ROC AUC score of each metric still in the variance margin of ROC AUC score of combination. However, for [FWW, RD], ROC AUC mean is similar or close to the ROC AUC of RD metric. When the lesion's volume superior to 10%, $\mathcal{MS}(thr > 10\%)$, the best scores of classification are approximately in [0.83,0.87] using [FWW, FA] and [Stick-AD, FWW].

Subset of 3 metrics: Figure. 5 shows also the mean and the variance of ROC AUC score for combination of 3 metrics firstly: [RD, MD, FA] and [FWW, MD, Stick-AD]. For these combinations, we remark that the ROC AUC mean of combination is better than ROC AUC score of each metric independently. For $\mathcal{MS}(thr > 10\%)$, [FWW, MD, Stick-AD] has ROC AUC mean in [0.82,0.86] and [RD, MD, FA] in [0.86, 0.90] which is an interesting result.

Subset of 4 metrics: In addition, we present two combination of 4 metrics: [RD, FWW, FA, MD] and [FWW, Stick-AD, MD, RD]. For $\mathcal{MS}(thr > 10\%)$, [RD, FWW, FA, MD] has ROC AUC mean in [0.84,0.86] and [FWW, Stick-AD, MD, RD] has ROC AUC mean in [0.87, 0.91].

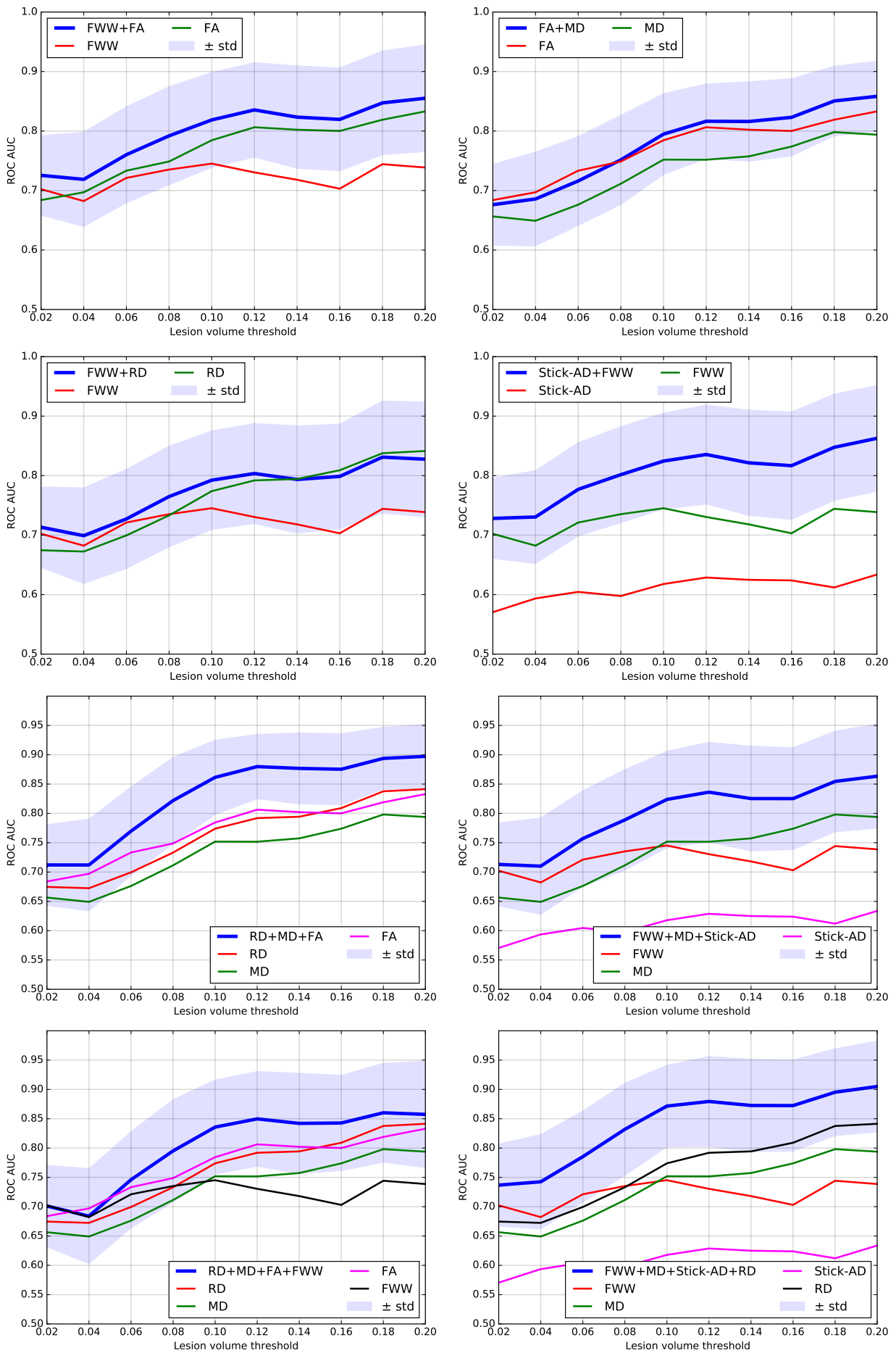


Figure 5: ROC AUC predicted by LDA for each combinations of metrics and ROC AUC of native metrics between MS patients and controls.

Data	Healthy Volunteers		MS patients								
	$\mathcal{V}_i (n=87)$		$\mathcal{N}AW\mathcal{M}_i (n=86)$			$\mathcal{M}S_i(5%) (n=36)$			$\mathcal{M}S_i(10%) (n=24)$		
Metric	Mean	STD	Mean	STD	p-value	Mean	STD	p-value	Mean	STD	p-value
FWW	0.1594	0.0431	0.1774	0.0672	0.0398	0.2076	0.0735	0.0007	0.2087	0.0641	0.0016
Stick-AD	0.0011	0.0003	0.0011	0.0003	0.3048	0.0010	0.0002	0.0378	0.0010	0.0003	0.0401
AD	0.0017	0.0002	0.0016	0.0003	0.2381	0.0017	0.0002	0.5844	0.0017	0.0002	0.1978
FA	0.6899	0.0800	0.6774	0.0941	0.3490	0.6150	0.0908	0.0001	0.6098	0.0667	1e-5
MD	0.0008	0.0001	0.0008	0.0002	0.8685	0.0009	0.0002	0.0071	0.0009	0.0001	8e-5
RD	0.0004	0.0001	0.0004	0.0002	0.5315	0.0005	0.0002	0.0008	0.0006	0.0001	3e-5

Table 3: For C2, C3 and C4 levels, mean and STD of each metric for healthy volunteers, for MS patients with or without lesions and for MS patients with lesion $>5\%$ and $>10\%$. **Dark green** means that p-value is inferior to 10^{-2} : there is a significant difference between healthy volunteers and MS patients. **weak green** means that p-value shows significant difference but $10^{-2} < \text{p-value} < 5 \cdot 10^{-2}$. n represents the number of vertebral level data available in [C2-C4] region.

To sum up, we can deduce that from all combinations, the combinations [RD, MD, FA] and [FWW, Stick-AD, MD, RD], which are overlaid in Figure. 6, give the best score of prediction between healthy volunteers and MS patients with lesion. The minimum of the variance margin for these subsets is close or slightly better to the best ROC AUC score of the independent RD or FA when the lesion’s volume superior to 10%.

5 Discussion and Conclusion

In this work, we have followed a pipeline that contains a collection of image processing and atlas-based approaches to extract the average diffusion MRI metrics per vertebral level in the cervical spinal cord. Diffusion measures involved are extracted from the diffusion tensor imaging and the Ball-and-Stick models. Then, we performed a statistical analysis to study their sensitivity associated with the presence and the evolution of MS lesions within the same vertebral level. This analysis includes an unpaired t -test and multivariate classification. Our cohort of spinal cord data was acquired on multiple clinical sites.

We showed that FWW, Stick-AD, FA, MD and RD have a significant difference between healthy volunteers and MS patients within the [C2-C4] region in the cervical spinal cord. Regarding FA, MD and RD, there are already showed in other studies involved in the spinal cord. [Valsasina et al. \(2005\)](#); [Agosta et al. \(2007a,b\)](#); [von Meyenburg et al. \(2013\)](#). However, we have many additions to them; firstly, the size of the data used to validate these results is relatively large. Secondly, 9 raters including radiologists and experienced readers who are segmenting MS lesions in anatomical scans which guarantee high accuracy. Thirdly, we quantify the diffusion measures within each vertebral level in the cervical spinal cord using an atlas-based approach. Fourthly, although it is a time-consuming task, we performed a strict quality check of each step of the pipeline as a crucial step for the quality of the analysis and the accuracy of the results.

Beyond our study using DTI metrics, we also investigated the sensitivity of multi-compartment models, in particular FWW and Stick-AD, to detect lesions in MS patients. We showed

that the Ball-and-Stick multi-compartment model can provide novel information about the evolution of tissue microstructure and should be included in the processing workflow. This also suggests that the acquisition protocol should be designed to enable richer multi-compartment models, including several b -values [Scherrer and Warfield \(2012\)](#). To our knowledge, only NODDI is the multi-compartmental diffusion models has been used to measure and investigate the microstructure and characterizing abnormalities in the spinal cord for MS patients [By et al. \(2017\)](#). But this study used only one slice of the cervical spine to investigate the sensitivity and feasibility of NODDI in patients with MS.

In our work, we performed a two-way analysis of variance between vertebral levels for each metric to illustrate the interaction term between them. We found that C2, C3, C4 vertebral levels show no significant inter-difference for all 6 diffusion metrics, as illustrated in Figure. 3. In fact, it was possible to pool [C2-C5] instead of [C2-C4] for FWW, Stick-AD, FA, MD and RD. However, for the MD metric, we found that the p-value between C3 and C5 equals 0.065, close to significant. Thus, we preferred to investigate the statistical analysis only within [C2-C4] interval.

Furthermore, another important contribution is that we explored a multivariate learning study to detect automatically the presence of an MS lesion using diffusion MRI data. Based on a selection of metrics extracted from diffusion MRI, we learned a linear classifier using LDA. The evaluation of the classification results was the ROC AUC. We manually select a set of measures with limited cross-correlation. We found that combining some metrics reaches up the prediction score of the presence of MS lesion and more performing than using each metric independently as shown in Figure. 5 and 6.

Therefore, we consider that a combination of 3 metrics [FA, RD, MD] and a combination of 4 metrics [FWW, MD, Stick-AD, RD] give the better ROC AUC score between healthy volunteers and MS patients with lesions. For MS patients with lesion’s volume between superior to 10%, [FA, RD, MD] combination has ROC AUC mean score in range [0.86, 0.90] and [FWW, Stick-AD, MD, RD] has ROC AUC mean in the range

[0.87, 0.91]. These intervals of prediction score demonstrate that the classification accuracy is good, and better than using each metric independently.

In conclusion, we demonstrated the grade of sensitivity to underlying microstructure changes in MS of each metric, including DTI and Ball-and-Stick reconstruction models in the context of a multicenter study. A multi-compartment model, Ball-and-Stick, can provide novel information about the MS damage to tissue microstructure. We showed also that choosing a subset of metrics, [FA, RD, MD] and [FWW, MD, Stick-AD, RD], which bring complementary information has significantly increased the prediction score of the presence of the MS lesion in the cervical spinal cord.

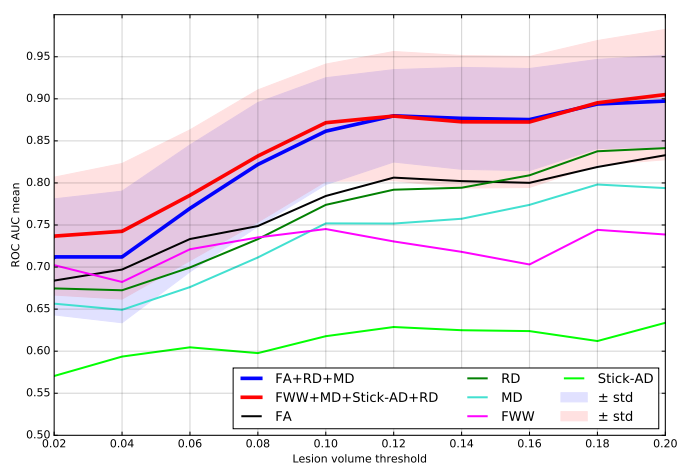


Figure 6: Overlays of ROC AUC score predicted by LDA for the best combinations: [FA, MD, RD] and [FWW, MD, Stick-AD, RD].

6 Declaration of Competing Interest

The authors declare that they have no known competing financial interests or personal relationships that could have appeared to influence the work reported in this paper.

References

Agosta, F., Absinta, M., Sormani, M., Ghezzi, A., Bertolotto, A., Montanari, E., Comi, G., and Filippi, M. (2007a). In vivo assessment of cervical cord damage in ms patients: a longitudinal diffusion tensor mri study. *Brain*, 130(8):2211–2219.

Agosta, F., Pagani, E., Caputo, D., and Filippi, M. (2007b). Associations between cervical cord gray matter damage and disability in patients with multiple sclerosis. *Archives of neurology*, 64(9):1302–1305.

Amélie, R., Anxionnat, R., Armspach, J.-P., Audoin, B., Barillot, C., Berry, I., Bonneville, F., Boutet, C., Castelnovo, G., Cervenansky, F., Cohen, M., Commowick, O., Cotton, F., De Seze, J., Dousset, V., Durand-Dubief, F., Edan, G., Ferre, J.-C., Galanaud, D., Glattard, T., Grand, S.,

Guillaumont, J., Guillevin, R., Guttmann, C., Hannoun, S., Heitz, F., Krainik, A., Kremer, S., Labauge, P., Menjot de Champfleury, N., Ranjeva, J.-P., Roch, J.-A., Sappey-Marinié, D., Savatovsky, J., Stankoff, B., Tourdias, T., Tourbah, A., and Vukusic, S. (2015). OFSEP, a nationwide cohort of people with multiple sclerosis: Consensus minimal MRI protocol. *Journal de Neuroradiologie / Journal of Neuroradiology*, 42(3):133 – 140.

Barkhof, F. (2002). The clinico-radiological paradox in multiple sclerosis revisited. *Current opinion in neurology*, 15(3):239–245.

Basser, P. J., Mattiello, J., and Lebihan, D. (1994). MR Diffusion Tensor Spectroscopy and Imaging. *Biophysical Journal*, 66:259–267.

Behrens, T., Berg, H. J., Jbabdi, S., Rushworth, M., and Woolrich, M. (2007). Probabilistic diffusion tractography with multiple fibre orientations: What can we gain? *Neuroimage*, 34(1):144–155.

Behrens, T. E., Woolrich, M. W., Jenkinson, M., Johansen-Berg, H., Nunes, R. G., Clare, S., Matthews, P. M., Brady, J. M., and Smith, S. M. (2003). Characterization and propagation of uncertainty in diffusion-weighted mr imaging. *Magnetic Resonance in Medicine: An Official Journal of the International Society for Magnetic Resonance in Medicine*, 50(5):1077–1088.

Bot, J. C. and Barkhof, F. (2009). Spinal-cord mri in multiple sclerosis: conventional and nonconventional mr techniques. *Neuroimaging clinics of North America*, 19(1):81–99.

By, S., Xu, J., Box, B. A., Bagnato, F. R., and Smith, S. A. (2017). Application and evaluation of noddif in the cervical spinal cord of multiple sclerosis patients. *NeuroImage: Clinical*, 15:333–342.

De Leener, B., Fonov, V. S., Collins, D. L., Callot, V., Stikov, N., and Cohen-Adad, J. (2018). Pam50: Unbiased multi-modal template of the brainstem and spinal cord aligned with the icbm152 space. *NeuroImage*, 165:170–179.

De Leener, B., Lévy, S., Dupont, S. M., Fonov, V. S., Stikov, N., Collins, D. L., Callot, V., and Cohen-Adad, J. (2017). Sct: Spinal cord toolbox, an open-source software for processing spinal cord mri data. *Neuroimage*, 145:24–43.

Filippi, M. and Grossman, R. I. (2002). Mri techniques to monitor ms evolution: the present and the future. *Neurology*, 58(8):1147–1153.

Grussu, F., Schneider, T., Zhang, H., Alexander, D. C., and Wheeler-Kingshott, C. A. (2015). Neurite orientation dispersion and density imaging of the healthy cervical spinal cord in vivo. *Neuroimage*, 111:590–601.

- Hesseltine, S., Law, M., Babb, J., Rad, M., Lopez, S., Ge, Y., Johnson, G., and Grossman, R. (2006). Diffusion tensor imaging in multiple sclerosis: assessment of regional differences in the axial plane within normal-appearing cervical spinal cord. *American Journal of Neuroradiology*, 27(6):1189–1193.
- Inglese, M. and Bester, M. (2010). Diffusion imaging in multiple sclerosis: research and clinical implications. *NMR in Biomedicine*, 23(7):865–872.
- Lévy, S., Benhamou, M., Naaman, C., Rainville, P., Callot, V., and Cohen-Adad, J. (2015). White matter atlas of the human spinal cord with estimation of partial volume effect. *Neuroimage*, 119:262–271.
- Miraldi, F., Lopes, F. C. R., Costa, J. V. A., Alves-Leon, S. V., and Gasparetto, E. L. (2013). Diffusion tensor magnetic resonance imaging may show abnormalities in the normal-appearing cervical spinal cord from patients with multiple sclerosis. *Arquivos de neuro-psiquiatria*, 71(9A):580–583.
- Ripley, B. (2002). Modern applied statistics with s.
- Rovaris, M., Judica, E., Gallo, A., Benedetti, B., Sormani, M., Caputo, D., Ghezzi, A., Montanari, E., Bertolotto, A., Mancardi, G., et al. (2006). Grey matter damage predicts the evolution of primary progressive multiple sclerosis at 5 years. *Brain*, 129(10):2628–2634.
- Ruthotto, L., Kugel, H., Olesch, J., Fischer, B., Modersitzki, J., Burger, M., and Wolters, C. (2012). Diffeomorphic susceptibility artifact correction of diffusion-weighted magnetic resonance images. *Physics in Medicine & Biology*, 57(18):5715.
- Scherrer, B. and Warfield, S. K. (2012). Parametric representation of multiple white matter fascicles from cube and sphere diffusion mri. *PLoS one*, 7(11):e48232.
- Snoussi, H., Caruyer, E., Cohen-Adad, J., Commowick, O., Combes, B., Bannier, E., Kerbrat, A., and Barillot, C. (2019). Geometric evaluation of distortion correction methods in diffusion mri of the spinal cord. In *IEEE International Symposium on Biomedical Imaging (ISBI)*.
- Stroman, P. W., Wheeler-Kingshott, C., Bacon, M., Schwab, J., Bosma, R., Brooks, J., Cadotte, D., Carlstedt, T., Ciccarelli, O., Cohen-Adad, J., et al. (2014). The current state-of-the-art of spinal cord imaging: methods. *Neuroimage*, 84:1070–1081.
- Valsasina, P., Rocca, M. A., Agosta, F., Benedetti, B., Horsfield, M. A., Gallo, A., Rovaris, M., Comi, G., and Filippi, M. (2005). Mean diffusivity and fractional anisotropy histogram analysis of the cervical cord in ms patients. *Neuroimage*, 26(3):822–828.
- von Meyenburg, J., Wilm, B. J., Weck, A., Petersen, J., Gallus, E., Mathys, J., Schaetzle, E., Schubert, M., Boesiger, P., von Meyenburg, K., et al. (2013). Spinal cord diffusion-tensor imaging and motor-evoked potentials in multiple sclerosis patients: microstructural and functional asymmetry. *Radiology*, 267(3):869–879.
- Wheeler-Kingshott, C., Stroman, P. W., Schwab, J., Bacon, M., Bosma, R., Brooks, J., Cadotte, D., Carlstedt, T., Ciccarelli, O., Cohen-Adad, J., et al. (2014). The current state-of-the-art of spinal cord imaging: applications. *Neuroimage*, 84:1082–1093.
- Xu, J., Shimony, J. S., Klawiter, E. C., Snyder, A. Z., Trinkaus, K., Naismith, R. T., Benzinger, T. L., Cross, A. H., and Song, S. (2013). Improved in vivo diffusion tensor imaging of human cervical spinal cord. *Neuroimage*, 67:64–76.
- Yushkevich, P. A., Piven, J., Hazlett, H. C., Smith, R. G., Ho, S., Gee, J. C., and Gerig, G. (2006). User-guided 3d active contour segmentation of anatomical structures: significantly improved efficiency and reliability. *Neuroimage*, 31(3):1116–1128.